J Appl Electrochem (2017) 47:573–581
DOI 10.1007/s10800-017-1061-6

RESEARCH ARTICLE

Anodic dissolution of vanadium in molten LiCl–KCl–$TiCl_2$

Ksenija Milicevic[1] · Bernd Friedrich[1] · Joachim Gussone[2] · Jan Haubrich[2]

Received: 11 October 2016 / Accepted: 23 February 2017 / Published online: 3 March 2017

Abstract The mechanism of anodic dissolution of pure vanadium in a titanium-enriched alkali chloride molten salt was investigated to determine whether it can be used as an ion source for a continuous Ti–V alloy deposition process. This study represents the first step towards the preparation of ternary Ti–Al–V alloys. Cyclic voltammetry as well electrochemical impedance spectroscopy (EIS) was performed and potentials for dissolution experiments were determined. Additionally, the influence of anode morphologies on the dissolution process, as a consequence of pretreatment, was investigated by scanning electron microscopy (SEM) and transmission electron microscopy (TEM). Results indicate that anodic vanadium dissolution is possible, but hindered by the electroless formation of a thin titanium layer. Additionally, a secondary reaction, namely the oxidation of Ti^{2+} ions, takes place, lowering the current efficiency of the process. Morphology investigations revealed the risk of grain detachment (material loss) from the vanadium electrode, which is critical in direct dissolution, whereas under indirect dissolution conditions, passivation impedes the controlled process. Thus, electrolysis is best carried out with coarse-grained vanadium electrodes in the direct dissolution range.

Graphical Abstract

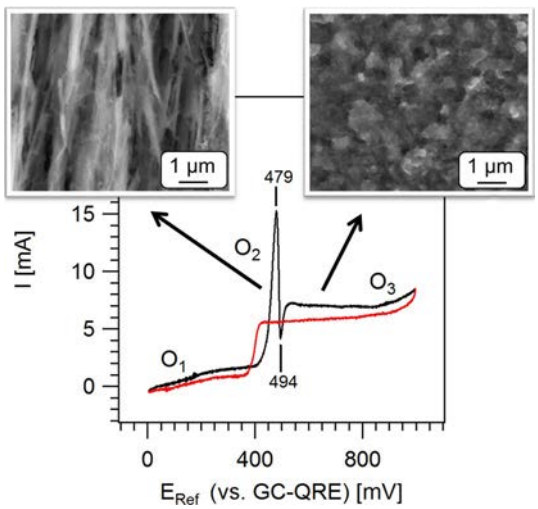

Keywords Titanium vanadium alloys · Anodic dissolution · Molten salt · Vanadium · Titanium · Indirect dissolution

1 Introduction

Vanadium is one of the most important alloying elements for use with titanium: as β-stabilizing element it improves strength, ductility and fabricability of titanium alloys [1]. It is commonly used in the production of α + β alloys such as Ti–6Al–4V or Ti–6Al–6V–2Sn that are used for compressor blades in turbines or in β-Ti alloys, e.g. Ti-10V-2Fe-3Al used for landing gears in the aerospace industry. Advanced applications enabled by these V-containing alloys also include titanium matrix composites (TMCs), which can offer very high specific strength and stiffness

✉ Ksenija Milicevic
kmilicevic@ime-aachen.de

[1] IME Process Metallurgy and Metal Recycling, RWTH Aachen University, Intzestr. 3, 52072 Aachen, Germany

[2] Institute of Materials Research, German Aerospace Center (DLR), Linder Höhe, 51147 Cologne, Germany

at temperatures up to 600 °C [2–4]. Titanium has been successfully deposited on SiC fibres [5], but the mechanical properties and oxidation resistance of pure titanium strongly limits its technical applicability.

Based on these results, the electrochemical deposition of the Ti alloys on SiC fibres seems promising, if the high production costs of techniques currently used [6] can be reduced. Different electrolyte systems have been considered and tested for synthesis of TMCs [7] and alkali metal chloride system based on LiCl–KCl has shown to be advantageous for compact coatings.

Electrochemistry of titanium species in LiCl–KCl electrolyte has been extensively researched [8–15], whereas there is very little research on the electrochemical behaviour of vanadium anodes in molten salts. Investigations on electrorefining vanadium anodes in LiCl–KCl began in the 1960s [16–22]. Furthermore, electronic absorption spectra of different vanadium species, particularly with a focus on the cathodic product, were studied [23–25]. More detailed research on electrode processes in halide melts has been carried out recently in the NaCl–KCl and other chloride systems [21, 26–29]. The behaviour of vanadium in the presence of titanium ions was investigated by Kazakova et al. without explanation of the dissolution mechanism, or mention of any difficulties occurring during dissolution [30]. Therefore, the driving force for this research is the understanding of this mechanism and how they affect the dissolution process.

2 Experimental

In all experiments, a eutectic mixture of LiCl–KCl was used as the base electrolyte, at a process temperature of approximately 430 °C. Additionally, in certain experiments, 2 wt% of $TiCl_2$ was added to this base electrolyte to study the influence of the Ti ions. All chemicals as well as electrodes and crucibles were stored and used under high purity argon atmosphere (O_2, H_2O <1 ppm) within a glovebox (Jacomex). KCl (Alfa Aesar, ACS, >99%) and LiCl (Alfa Aesar, ACS, >99%) referred as standard chemicals further in text, were dried separately for 3 days at 200 °C and 300 °C, respectively [7]. Moreover, high purity KCl (Alfa Aesar, ultra dry, 99.95% metals basis) and LiCl (Alfa Aesar, ultra dry, 99.9% metals basis) were used without further treatment. For the titanium containing electrolytes, $TiCl_2$ (Sigma-Aldrich, 99.98% anhydrous) was added prior to melting the salt mixture.

The molten salt reactor was attached to the base plate of the main (working) space of the glovebox via a gas-tight connection in order to minimize the contamination of the system, especially water pick up of the highly hygroscopic chemicals or the introduction of oxygen.

A miniature experimental setup with thin electrodes and small amounts of salts (approx. 10 g) was employed for this study. As working electrodes (WE) or quasi-reference electrodes (QRE) vanadium wires (Ø = 0.25, 0.5 and 1.0 mm, respectively, with purity >99.5%) were used. Glassy carbon (GC) crucibles served as the reference electrode (QRE) while a tungsten wire (Ø = 0.5 mm, 99.95%) was used as counter electrode (CE). Tungsten electrodes were electrochemically polished in dilute KOH solution (ca. 0.3 mol/L) and cleaned with deionized water. Different pre-treatments were chosen for preparation of the vanadium wires: after etching with diluted HF (ca. 0.25 mol/L) some electrodes were additionally electro-polished in HCl solution (0.6 mol/L, 6 V, 30 s) [31] to investigate the influence of the surface morphology on dissolution behaviour. Vanadium wires were annealed at 900 °C for approx. 2 h, to study the effect on the microstructure. All electrochemical measurements were carried out with a *BANK HC400* potentiostat/galvanostat. For impedance spectroscopy, a *Zahner Zennium* electrochemical workstation was used.

After the experiments, electrodes were cleaned with deionized water and subsequently dried. Their microstructures and morphologies were investigated using *Zeiss Ultra 55* scanning electron microscope (SEM) and *Philips Tecnai F30* transmission electron microscope (TEM). Both systems were equipped with energy dispersive X-ray spectroscopy (EDS). The lamella for the TEM investigation was prepared by focussed ion beam (FIB: *FEI, Helios Nanolab 650*).

3 Results and discussion

3.1 Tests for corrosion at open-circuit potential

To prove the stability of the vanadium wires at zero current, their corrosion behaviour was tested by dipping vanadium wires in LiCl–KCl or LiCl–KCl–$TiCl_2$ for 30 min at 430 °C. SEM analysis showed no changes in the surface morphology of the vanadium wires after corrosion testing in pure LiCl–KCl, although the presence of titanium ions in LiCl–KCl–$TiCl_2$ led to the deposition of a significant amount of titanium on the surface of the vanadium wires (EDS spectra showed up to >30 wt% Ti).

The formation of a titanium-rich layer on the vanadium electrodes may take place according to the following disproportionation reaction (Eq. 1):

$$3TiCl_2 + V = Ti{-}V + 2TiCl_3 \quad (1)$$

The alloy (Ti–V) formation at the upper surface of the vanadium electrode is assumed to provide a driving force for the reaction.

3.2 Electrochemical measurements

Cyclic voltammetry (CV) measurements with vanadium working electrodes were carried out in both melts (LiCl–KCl and LiCl–KCl–$TiCl_2$) to analyse the occurring processes.

3.2.1 Electrolyte without $TiCl_2$ addition

The CV measurements with vanadium working electrode in LiCl–KCl without $TiCl_2$ addition were conducted with a rather large potential range (1200 mV). They were repeated with the standard chemicals (as defined in the experimental part) and also with the ultra-dry LiCl–KCl chemicals (measurements shown here) and remained consistent. The oxidation half-cycle of the CV shown in Fig. 1 can be split into several regions:

(i) current increases up to 305 mV (O_1),
(ii) subsequent drop to a sharp minimum at 317 mV, followed by an increase to
(iii) plateau up to ca. 800 mV, and
(iv) rise to a maximum value at 1004 mV (O_2) followed by
(v.) current breakdown and a sharp minimum similar to that observed at 315 mV.

The current increase (O_1) in region (i) corresponds to the direct dissolution reaction of vanadium according to Eq. 2:

$$V(0) \rightarrow V^{2+} + 2e^- \quad (2)$$

In the current plateau region (iii) between ca. 315 and 800 mV, the anodic current is limited by the formation of a passivation layer. A possible explanation for this phenomenon is a diffusion inhibition of the V^{2+} ions formed by Eq. 2 from the electrode: the diffusion layer supersaturates and an undissolved product is formed.

The comparatively high current at the peak of O_1 (13 mA) causes an excess of V(II) species to form and the current drops below the limiting current of indirect dissolution (region ii, minimum at 317 mV), before an equilibrium between the formation and dissolution rates of the undissolved product determines the value of the limiting current (plateau between 315 and around 800 mV). Such a steep current drop has already been observed in aqueous electrolytes and is considered indicative of passivation [32]. The current increase in region (iv) starting at about 800 mV peaking at 1004 mV is considered to be due to V^{3+} ions being formed according to Eq. 3, allowing for a higher charge transfer per atom (corresponding to higher current):

$$V^{2+} \rightarrow V^{3+} + e^- \quad (3)$$

Once again, after the peak at 1004 mV a sharp drop occurs (region v), which implies another passivation process on the vanadium electrode surface caused by enrichment of the V^{3+} species. During the current increase (region iv), the chemistry of the passivation layer changes until at ca. 1004 mV it consists completely of trivalent vanadium species.

The reverse scan of the CV can also be split into several distinct regions. The first region here is marked by de-passivation phenomena at around 990, 980 and

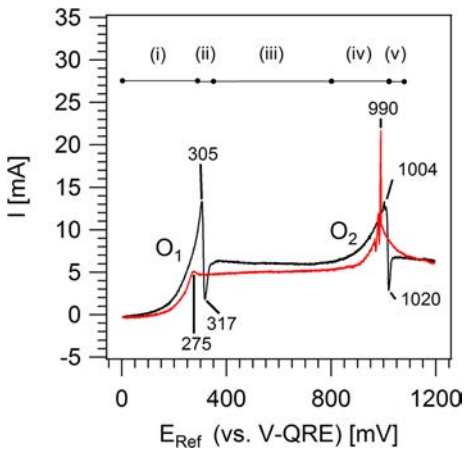

Fig. 1 Cyclic voltammetry in eutectic LiCl–KCl at ca. 700 K with $v = 0.01$ V/s. During the oxidation cycle (*black line*), the formation of divalent (O_1) and trivalent (O_2) vanadium species can be observed. The current plateau between both *sharp peaks* can be explained by passivation. The reduction cycle (*red line* in online version) is mainly shaped by de-passivation phenomena (positive current spikes)

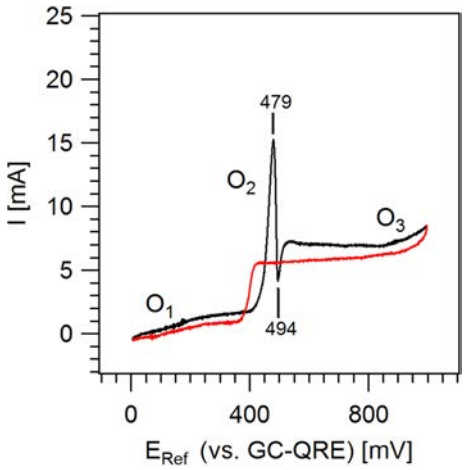

Fig. 2 Cyclic voltammetry in LiCl–KCl—2 wt% $TiCl_2$ at ca. 700 K with $v = 0.01$ V/s. During the oxidation cycle (*black line*) the oxidation of Ti^{2+} (O_1) and vanadium (O_2) can be observed. During the reduction cycle (*red line* in online version), a crossover was observed which may be explained by the fact that the dissolution of vanadium is shifted to more positive potentials because of the presence of titanium on the surface of the electrode

960 mV, when short but drastic current breakthroughs are observed. At ca. 275 mV, another, much less pronounced current increase indicates a passivation layer of much higher stability. In this study, it was not possible to ascertain which undissolved products the passivation layers consisted of (this could be achieved with in-situ spectroscopy methods [33–36]). However, it is reasonable to assume complexes such as $KVCl_3$ or K_2VCl_4 in the case of the divalent vanadium ions and $KVCl_4$ or K_3VCl_6 for trivalent vanadium, as it was demonstrated by absorption spectroscopy that these complexes exist in KCl containing molten salts [23–25, 37].

Additionally, the phase diagrams show that increasing the concentrations of VCl_2 [38] or VCl_3 [39], the aforementioned complexes form at lower temperatures.

3.2.2 *Electrolyte with $TiCl_2$ addition*

Conversely, the CV measurements in LiCl–KCl–$TiCl_2$ showed a similar behaviour, but with vanadium dissolution shifted to more anodic potentials and a crossover during the return scan (Fig. 2). Here a measurement with a potential range of ca. 1000 mV is shown because at more positive potentials, a very similar behaviour to the LiCl–KCl scenario was found. Initially, the current increases much smoother, but towards the peak O_2 at 479 mV it is much steeper than in the case of the pure LiCl–KCl electrolyte. The current increase (O_1) beginning already at 0 mV can be attributed to the oxidation of divalent Ti ions according to Eq. 4:

$$Ti^{2+} \rightarrow Ti^{3+} + e^- \quad (4)$$

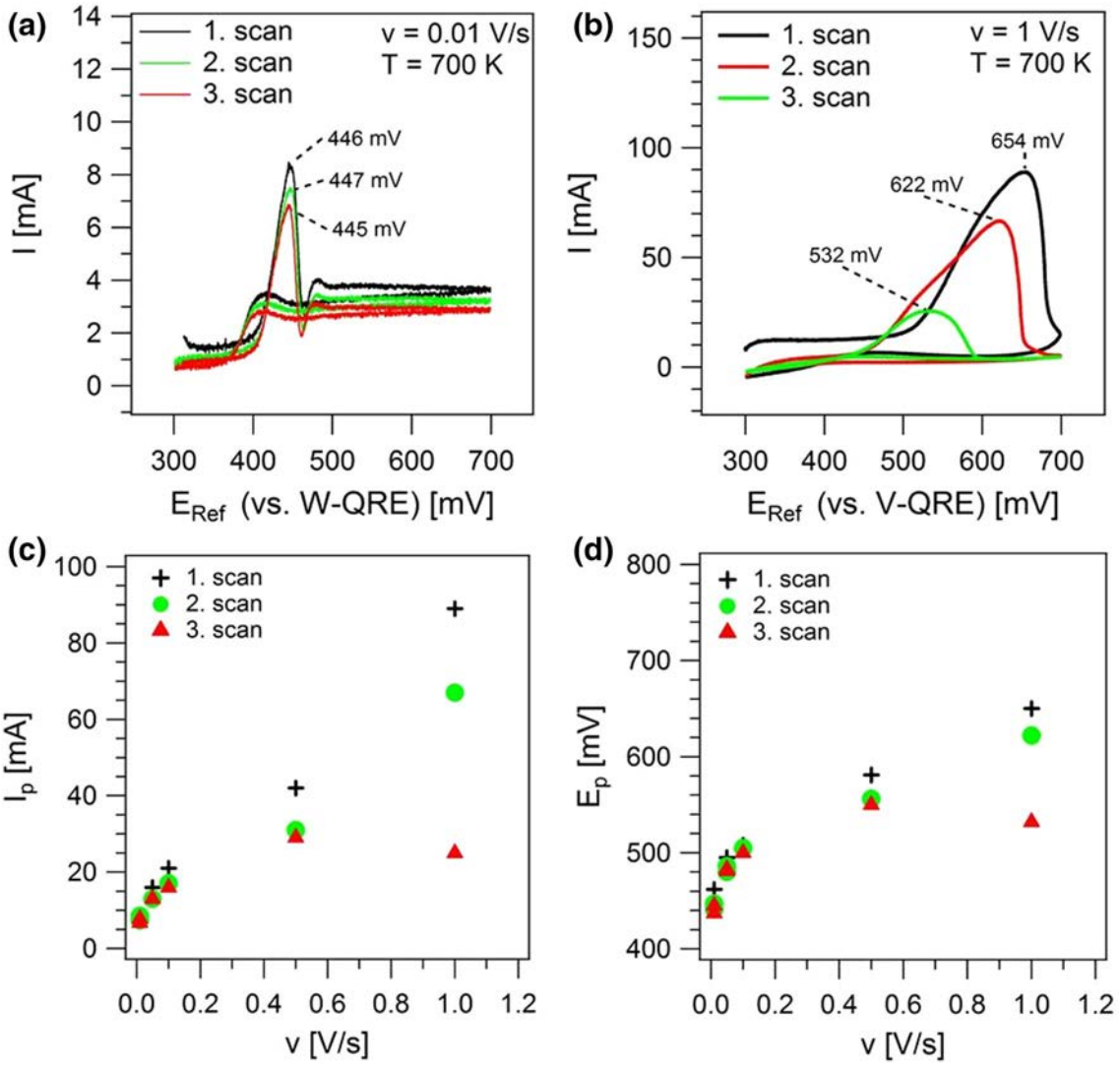

Fig. 3 Cyclic voltammetry carried out in the potential range between 300 and 700 mV in LiCl–KCl- 2 wt% $TiCl_2$ at ca. 700 K. **a** Three subsequent CV scans with $v = 0.01$ V/s. **b** Three subsequent CV scans with $v = 1$ V/s. **c** Peak current values (I_p) for repeated CV scans versus different scan rates ($v = 0.01$–1 V/s). **d** Peak potential values (E_p) for repeated CV scans versus different scan rates ($v = 0.01$–1 V/s)

During the oxidation cycle, the oxidation of Ti^{2+} (O_1) and vanadium (O_2) can be observed. During the reduction cycle, a crossover was observed which may be explained by the fact that the dissolution of vanadium is shifted to more positive potentials in the presence of titanium, on the surface of the electrode.

This crossover may be linked to the formation of a thin titanium-rich layer (as described in Sect. 3.1) that was not present in the case of the Ti-free LiCl–KCl electrolyte system (Fig. 1). The titanium-rich layer impedes vanadium dissolution, whereupon the current rises steeply up to the point that passivation takes place. In contrast, during the reverse scan, there is no titanium-rich layer on the surface and the dissolution range is extended to more negative potentials (crossover).

For the system with Ti^{2+}, scan rate was varied for the potential range between 300 and 700 mV to study vanadium dissolution process in detail. Three CV measurements

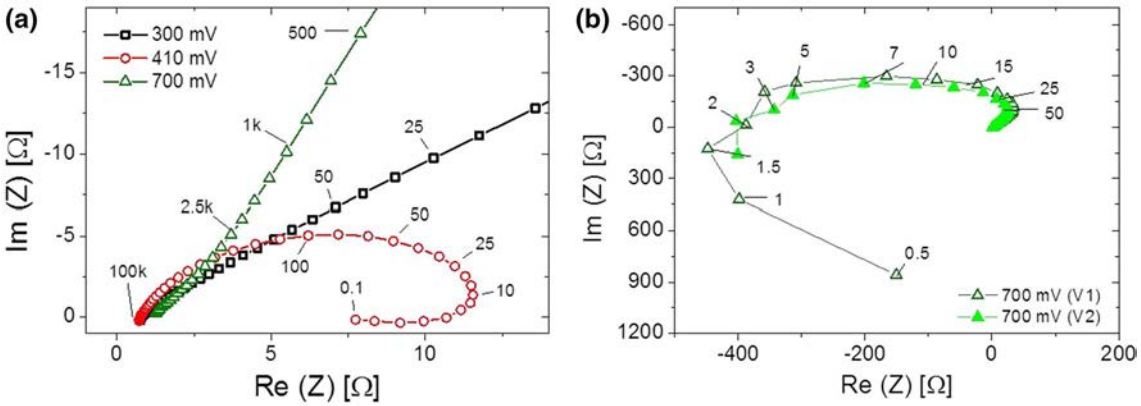

Fig. 4 Impedance measurements carried out with vanadium anode in LiCl–KCl–$TiCl_2$ at potentials corresponding to oxidation of Ti^{2+} (300 mV), direct dissolution (410 mV) and indirect dissolution of vanadium (700 mV). Frequency was varied from 0.1 Hz to 100 kHz

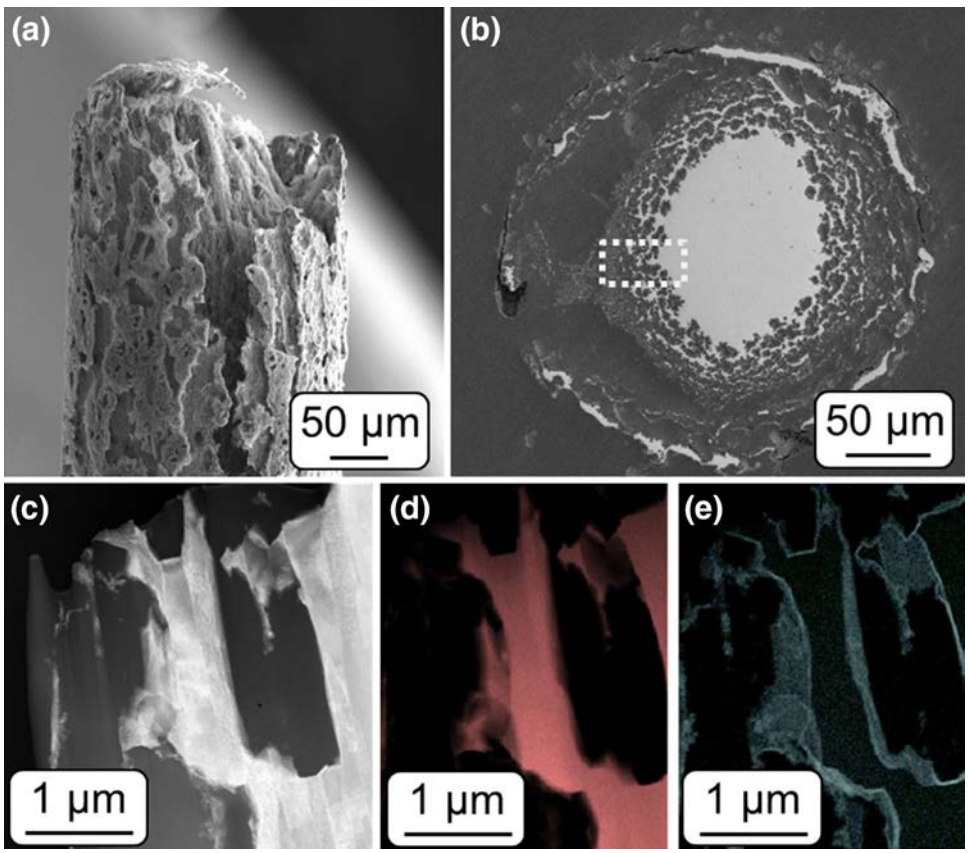

Fig. 5 Investigation of vanadium dissolution in LiCl–KCl-2 wt% $TiCl_2$. **a** SEM image of V electrode. **b** Cross section with extraction point of lamella (*framed with white dotted line*). **c** Dark field TEM image of region of interest. **d** EDS mapping of vanadium. **e** EDS mapping of titanium

were carried out, one directly after another. The CV obtained at low scan rates (Fig. 3a) showed a good reproducibility, i.e. the potential and the current progressions are very similar for each scan. In contrast, at high scan rates (Fig. 3b) the peak potentials and peak currents decreased significantly at each repetition. The deviation starts when the scan rates exceed 0.5 V/s (Fig. 3c, d). This behaviour can be attributed to the fact that passivation/inhibition layers do not dissolve completely before the subsequent scan starts, which is a further confirmation of its existence. It also indicates that it dissipates kinetically delayed.

In order to gain further insight into the rate-limiting steps of these processes, impedance spectroscopy was carried out at three relevant potentials (300, 410, 700 mV). In the Nyquist plot for 300 mV (Fig. 4a), we observed a diffusion-controlled behaviour (Warburg impedance) [40] corresponding to the oxidation of Ti^{2+} (O_1, see Eq. 4). At 410 mV, the semicircle indicates that the direct dissolution (O_2, Eq. 2) of V is charge transfer controlled [41]. At 700 mV (Fig. 4b) within the current plateau region (indirect dissolution), a typical behaviour for passivation, i.e. a large circular curve extending to negative ohmic resistances (Fig. 4b), is detected, which again qualitatively confirms the existence of passivation layer. A detailed consideration of a similar impedance behaviour can be found in the work of Sadowsky et al. [32].

3.3 Characterisation of the vanadium anodes

Intense corrosion was found on vanadium wires tested in the direct dissolution range. Vanadium wires that were simply cleaned in deionized water, or etched in diluted HF (pre-treatment), exhibited deep holes that extended under the surface of an outer titanium-rich layer (Fig. 5a). EDS results (ca. 4 wt% Ti) are only semi-quantitative and indicative, because of the sample geometry (no plain surface) and the limited thickness (Ti content not homogeneous within the excitation volume).

In order to gain further insight into the structure and thickness of the titanium layer, a lamella for TEM investigations was prepared with FIB from a cross section shown in Fig. 5b. EDS measurements carried out within the TEM,

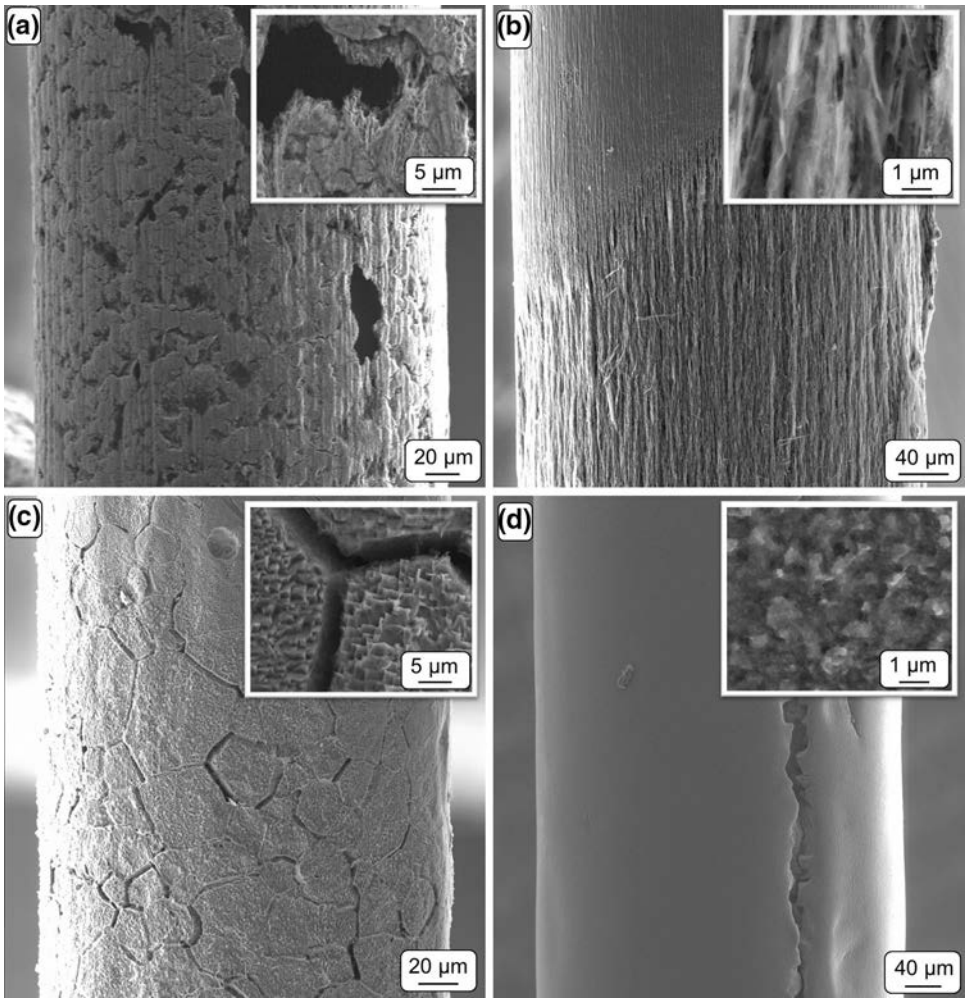

Fig. 6 SEM images of vanadium electrodes after dissolution in LiCl–KCl–$TiCl_2$. Electrolyses carried out in the direct dissolution range ($E \approx 400$ mV) led to rough surfaces (**a**–**c**). In contrast electrolyses in the indirect dissolution range ($E \approx 700$ mV) cause very smooth surfaces (**d**). Please note that electrodes with different diameters were used: Ø 0.25 mm (**a, c**), Ø 0.5 mm (**b, d**)

demonstrate that the titanium-rich layer was evenly distributed on the extremely fine structures around the remaining vanadium core of the electrode. The thickness of the layer differs in this part of the electrode between a few to a few hundred nanometres (EDS-mappings of vanadium and titanium in Fig. 5d, e).

For the dissolution experiments described in the following section, ultra-dry chemicals were used to minimize the influence of impurities, especially those resulting from hydrolysis. An overview demonstrating the influence of the pre-treatment, i.e. the initial state of the electrode, on the dissolution is shown in Fig. 6. Electrodes with a fissured surface layer resulting from the wire drawing process exhibit large holes after the experiment in the direct dissolution range (Fig. 6a). The image shows the beginning of a process leading to a disintegration of the electrode as shown in Fig. 5.

Electrodes studied were electrochemically polished prior to test work to minimize any preferential corrosion in rough areas or pits. The surface of the dipped part is fibre-structured and partly elongated grains protrude as if burst from inside (Fig. 6b). This can be explained by the residual stresses introduced by the wire drawing process. Such behaviour renders these electrodes unsuitable for a well-controlled, stable dissolution process, since grains separate from the electrode without being dissolved in the electrolyte due to the ongoing disintegration process.

One possible approach to resolve this issue might be annealing of the vanadium electrodes before the electrolyses. This reduces residual stresses and creates a coarser microstructure. For example, vanadium wires annealed at 900 °C demonstrate that the dissolution takes place preferentially at the boundaries of the recrystallized globular grains (Fig. 6c). However, there is also orientation dependence in the dissolution of different crystal planes. Since dissolution is significantly faster at grain boundaries, material loss from the electrode can reduce the efficiency of the dissolution process, when grains detach from the electrode even in the case of a coarse microstructure. An explanation for this might be that the titanium-rich layer, which was ca. 2–4 at.% in the experiments carried out in the direct dissolution range, inhibits the dissolution process. In holes or undercuts, however, there is a depletion of Ti ions in the electrolyte, and as soon as there is a titanium-free vanadium surface, dissolution can take place at lower potentials.

Finally, the morphology of electrodes in the indirect dissolution range was investigated. In contrast to all experiments carried out within the direct dissolution

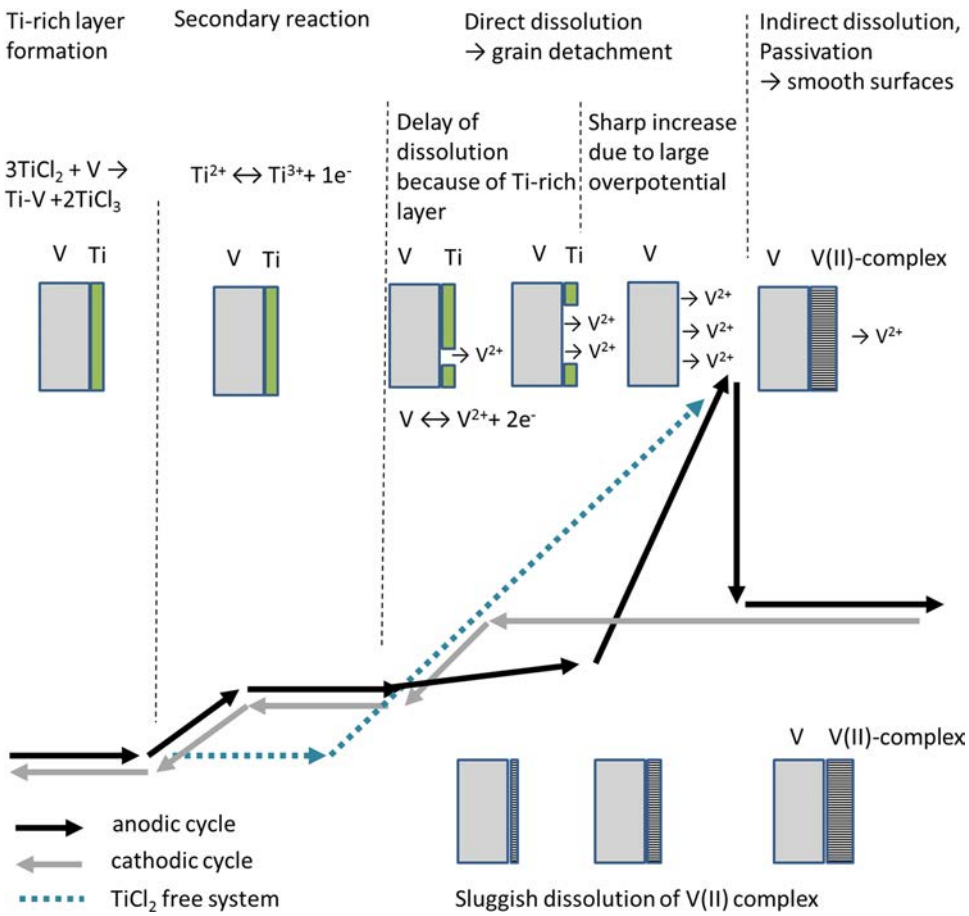

Fig. 7 Comparative schematic representation of the dissolution mechanisms in LiCl–KCl and LiCl–KCl–$TiCl_2$

range, a very smooth surface was obtained (Fig. 6d). At very high magnification, a submicrometre-sized crystal-like surface morphology was observed. The indirect dissolution is basically an electropolishing process. While during direct dissolution, the process takes place preferentially in holes or at grain boundaries, the passivating layer inhibits the removal at undercuts whereas protrusions are preferred. The surface of these electrodes contained significantly less titanium (<1 at.%) than the electrodes which underwent direct dissolution, indicating there was a titanium-free surface. The low titanium content observed with EDS formed immediately after the electrolysis, but before the electrode was taken out of the electrolyte (ca. 1 s). However, the drawback of indirect dissolution is the fact that it cannot be galvanostatically controlled, which is a requirement for the targeted electrolysis process.

The comparative schematic representation of the dissolution mechanisms in both electrolyte systems (LiCl–KCl and LiCl–KCl–$TiCl_2$) is shown in Fig. 7. Experimental results illustrate that dissolution mechanism is complicated by several factors:

1. The current efficiency of the dissolution process is supposed to be reduced because of the concurrent oxidation of Ti^{2+} ions (O_2, Fig. 2).
2. The direct dissolution process takes place preferentially at the grain boundaries, which can cause material loss when grains separate from the electrode. This is especially critical for vanadium electrodes with very fine microstructures. In contrast, the indirect dissolution process causes a very smooth surface morphology.
3. At high current densities, the vanadium electrode is passivated. The surface of the electrode becomes very smooth but the process cannot be controlled galvanostatically.

4 Conclusion and outlook

The anodic dissolution of vanadium in LiCl–KCl–$TiCl_2$ was investigated via electrochemical measurements, as a first step for the development of a Ti–V–Al alloy electrodeposition process. The anode morphology was affected by the applied potential and the pre-treatment of the electrode. The findings demonstrate that electrolysis should be carried out in the direct dissolution range with coarse-grained vanadium electrodes. Further studies will focus on investigating the current efficiency of vanadium dissolution in direct dissolution area.

Acknowledgements The German Research Foundation is gratefully acknowledged for their financial support for this project (HA 4397/6-1).

References

1. Donachie MJ (2000) Titanium: a technical guide, 2nd edn. ASM International, Materials Park
2. Leyens C, Hausmann J, Kumpfert J (2003) Continuous fiber reinforced titanium matrix composites: fabrication, properties, and applications. Adv Eng Mater 5(6): 399–410. doi:10.1002/adem.200310093
3. Ward-Close CM, Chandrasekaran L, Robertson JG, Godfrey SP, Murgatroyd DP (1999) Advances in the fabrication of titanium metal matrix composite. Mater Sci Eng A 263(2):314–318. doi:10.1016/S0921-5093(98)01162-9
4. Gofrey TMT, Goodwin PS, Ward-Close CM (2000) Titanium particulate metal matrix composites—Reinforcement, production methods and mechanical properties. Adv Eng Mater 2(3):85–91. doi:10.1002/(SICI)1527-2648(200003)2:3<85:AID-ADEM85>3.0.CO;2-U
5. Gussone JG, Hausmann JM (2011) Deposition of titanium on SiC fibres from chloride melts. J Appl Electrochem 41(6):657–662. doi:10.1007/s10800-011-0284-1
6. Vassel A (1999) Continuous fibre reinforced titanium and aluminium composites: a comparison. Mater Sci Eng A 263(2):305–313. doi:10.1016/S0921-5093(98)01161-7
7. Gussone JG (2012) Production of titanium matrix composites by electrolytic deposition of titanium on reinforcing fibers. Dissertation, RWTH Aachen University **(in German)**
8. Rolland WK (1987) Electrodeposition of titanium from alkali chloride melts contining di- and tri-valent titanium chloride. Dissertation, NTNU Trondheim
9. Haarberg GM, Rolland W, Sterten A, Thonstad J (1993) Electrodeposition of titanium from chloride melts. J Appl Electrochem 23(3). doi:10.1007/BF00241912
10. Lantelme F, Kuroda K, Barhoun A (1998) Electrochemical and thermodynamic properties of titanium chloride solutions in various alkali chloride mixtures. Electrochim Acta 44(2–3):421–431. doi:10.1016/S0013-4686(98)00168-6
11. Girginov A, Tzvetkoff TZ, Bojinov M (1995) Electrodeposition of refractory metals (Ti, Zr, Nb, Ta) from molten salt electrolytes. J Appl Electrochem 25(11):993–1003. doi:10.1007/BF00241947
12. Haarberg GM, Kjos OS, Martinez AM, Osen KS., Skybakmoen E, Dring K (2010) Electrochemical behavior of dissolved titanium species in molten salts. In: 218th ECS meeting. ECS, pp 167–173
13. Popov BN, Kimble MC, White RE, Wendt H (1991) Electrochemical behaviour of titanium(II) and titanium(III) compounds in molten lithium chloride/potassium chloride eutectic melts. J Appl Electrochem 21(4):351–357. doi:10.1007/BF01020221
14. Zhu X, Wang Q, Song J et al (2014) The equilibrium between metallic titanium and titanium ions in LiCl–KCl melts. J Alloy Compd 587:349–353. doi:10.1016/j.jallcom.2013.09.151
15. Song J, Wang Q, Zhu X et al (2014) Thermodynamic properties of different titanium ions in fused LiCl–KCl eutectic. In: Neelameggham NR, Alam S, Oosterhof H et al (eds) Rare metal technology 2014. Wiley, Hoboken, pp 133–138
16. Voleinik VV, Kunaev AM (1963) Anodic polarisation of vanadium in chloride melts. Vestnik Akademii Nauk Kazachskoj SSR 19(7):41–48 (**in Russian**)

17. Lei KPV, Sullivan TA (1971) Electrorefining of vanadium prepared by carbothermic reduction of V_2O_5. Metall Mater Trans B 2(8):2312–2314. doi:10.1007/BF02917579
18. Lei KPV, Sullivan TA (1968) High-purity vanadim. J Less Common Met 14(1):145–147. doi:10.1016/0022-5088(68)90212-9
19. Sullivan TS (1965) Electrorefining vanadium. J Met 17:45–48
20. Lei KP (1967) An electrolytic process for producing ductile vanadium. U.S. Department of Interior Bureau of Mines, Washington DC
21. Baker DH, Ramsdell JD (1960) Electrolytic vanadium and its properties. J Electrochem Soc 107(12):985–989
22. Molina R (1961) Chemical properties of some elements in eutectic molten lithium chloride-potassium chloride. Dissertation, University of Paris **(in French)**
23. Gruen DM, McBeth RL (1962) Absorption Spectra of the II, III, IV and V oxidation states of vanadium in LiCl–KCl eutectic. Octahedral-tetrahedral transformations of V(II) and V(III). J Phys Chem 66(1):57–65. doi:10.1021/j100807a012
24. Chernyshov MV, Polovov IB, Volkovich VA, Vasin BD, Rebrin OI, Vinogradov KV, Griffiths TR (2010) Electronic absorption spectra of vanadium species in halide melts. In: 218th ECS meeting. ECS, pp 287–296
25. Polovov IB, Volkovich VA, Shipulin SA, Maslov SV, Khokhryakov AA, Vasin BD, Griffiths TR, Thied RC (2003) Erratum to "Chemistry of vanadium chlorides in molten salts: an electronic absorption spectroscopy study". J Mol Liq 105(1):105–116. doi:10.1016/S0167-7322(03)00025-4
26. Polovov IB, Tray ME, Chernyshov MV, Volkovich VA, Vasin BD, Rebrin OI (2014) Electrode processes in vanadium-containing chloride melts. In: Gaune-Escard M, Haarberg GM (eds) Molten salts chemistry and technology. Wiley, Hoboken, pp 257–281
27. Tripathy PK, Sehra JC, Bose DK, Singh RP (1996) Electrodeposition of vanadium from a molten salt bath. J Appl Electrochem 26(8):887–890. doi:10.1007/BF00683752
28. Polovov IB, Vasin BD, Abakumov AV, Rebrin OI, Chernyshov MV, Volkovich VA, Griffiths TR (2006) Thermodynamics of the formation of vanadium(II) complexes in chloride melts. In: 210th ECS Meeting, Cancun, Mexico
29. Chernyshov MV, Polovov IB, Nechkin GA, Volkovich VA, Rebrin OI, Rylov AN (2008) Vanadium electrorefining in NaCl–KCl based melts. In: Proceedings of 2008 joint symposium on molten salts, pp 752–756
30. Kazakova OS, Kuznetsov SA (2013) Electrochemical behavior and electrorefining of vanadium in melts containing titanium salts. ECS Trans 50(11): 181–190. doi:10.1149/05011.0181ecst
31. Petzow G, Carle V (2006) Metalographic, ceramographic, plastographic etching. Borntraeger, Berlin (**in German**)
32. Sadkowski A, Dolata M, Diard JP (2004) Kramers–Kronig transforms as validation of electrochemical immittance data near discontinuity. J Electrochem Soc 151(1):E20. doi:10.1149/1.1633270
33. Iwasita T, Nart FC (1997) In situ infrared spectroscopy at electrochemical interfaces. Prog Surf Sci 55(4):271–340. doi:10.1016/S0079-6816(97)00032-4
34. Chang KC, Yildiz B, Myers JD, Carter JD, You H (2008) In situ synchrotron X-ray spectroscopy of lanthanum manganite solid oxide fuel cell electrodes. In: 214th ECS meeting, Honolulu, Hawai
35. DeCaluwe SC, Grass ME, Zhang C, Gabaly FE, Bluhm H, Liu Z, Jackson GS, McDaniel AH, McCarty KF et al (2010) In situ characterization of ceria oxidation states in high-temperature electrochemical cells with ambient pressure XPS. J Phys Chem C 114(46):19853–19861. doi:10.1021/jp107694z
36. Seifert F, Paris E, Dingwell DB, Davoli I, Mottana A (1993) A high-temperature device for in situ measurement of X-ray adsorption spectra. Condens Matter Mater Commun 1(2):115–121
37. Rebrin OI, Scherbakov RY, Polovov IB, Mihalev SM, Volkovich VA, Muhamadeev AS, Vasin BD (2002) Investigation of the kinetics of electrode processes in halide melts containing beryllium, vanadium, niobium and hafnium. Electrochem Soc Proc 19:460–472
38. Seifert HJ, Ehrlich P (1960) About the systems NaCl/VCl_2, KCl/VCl_2 und CsCl/VCl_2 (in German). J Inorg Gen Chem 302(5–6):284–288. doi:10.1002/zaac.19603020506
39. Shchukarev SA, Perfilova IL (1963) Reaction of vanadium trichloride with sodium, potassium and rubidium chlorides. Russ J Inorg Chem 8(9):1100–1102
40. Macdonald JR, Kenan WR (1987) Impedance spectroscopy: emphasizing solid materials and systems. Wiley, New York
41. Lvovich VF (2012) Impedance spectroscopy: applications to electrochemical and dielectric phenomena. Wiley, Hoboken